Original scientific paper

DESIGN AND OPTIMIZATION OF THE VARIABLE-DENSITY LATTICE STRUCTURE BASED ON LOAD PATHS

Fenghe Wu[1], Hui Lian[1], Guobin Pei[1], Baosu Guo[1], Zhaohua Wang[2]

[1]School of Mechanical Engineering, Yanshan University, Qinhuangdao, China
[2]School of Mechanical Engineering,
Taiyuan University of Science and Technology, Taiyuan, China

Abstract. *Lattice structure is more and more widely used in engineering by replacing solid structure. But its mechanical performances are constrained by the external shape if the unit cells are directly filled in the design domain, and the traditional topology optimization methods are difficult to give the explicitly mechanical guidance for the distribution of internal unit cells. In this paper, a novel design and optimization method of variable-density lattice structure is proposed in order to simultaneously optimize the external shape and the internal unit cells. First of all, the envelope model of any given structure should be established, and the load paths need to be visualized by the theory of load path. Then, the design criteria of external shape are established based on the principle of smoother load paths in the structure. An index of load flow capacity is defined to indicate the load paths density and to control the density distribution of unit cells, and a detailed optimization strategy is given. Finally, three examples of a cantilever plate, an L-shaped bracket and a classical three-point bending beam are used to verify the method. The results show that the models designed by the proposed method have better mechanical performances, lower material usage and less printing time.*

Key Words: *Lattice Structure, Load Paths, Additive Manufacturing, Optimization*

1. INTRODUCTION

Lattice Structure (LS) is a kind of cellular structure composed of a large number of unit cells arranged in a specific manner, which has some excellent performances including high strength relative to low mass, good energy absorption and high thermal and acoustic insulation [1-3]. Some multifunctional usages of cellular structures in all scales ranging from nanometers to centimeters or even larger have been reported in recent literature [4-5].

Additive manufacturing (AM) technology further promotes the application of LS in engineering by building engineering components in a bottom-up, layer-by-layer manner as opposed to traditional subtractive manufacturing such as milling, turning, forging, and so on [6, 7]. For example, an aero-bracket with the LS features was designed and manufactured using different types of AM processes and the weight of initial model is reduced by 50% [8]. Therefore, it is a trend that the solid structure is replaced by the corresponding LS to improve the mechanical performances and achieve a lightweight design in the future.

Generally, the design domain of the solid structure is directly filled with uniform-density unit cells [9], and the mechanical performances of the LS model are verified by simulation and experiment. But, in fact, different regions in a given structure usually bear different magnitude of loads [10, 11], while the mechanical performances of uniform-density lattice structures still have the potential to be improved, which depends on the topology, shape, size and orientation of the unit cell [1]. By controlling these variables, LS can be modified in space to improve the performances such as stiffness or strength [12-15]. In the following section, some existing research studies about the design, analysis and optimization of variable-density LS are reviewed and discussed.

A global relative density mapping method for the design of non-uniform LS is proposed in references [16-17], which introduces the topology optimization method into the LS design. The diameter of unit cells is changed through the linear interpolation results of continuum topology optimization to reduce the weight and improve the performances. Zhang et al. [18] proposed an efficient design-optimization of variable-density hexagonal cellular structure based on three key techniques: homogenization, optimization, and construction (HOC). Then, the variable-density topology optimization of LS considering stress constraints, structural dynamic characteristics and heat conduction problems are studied in references [19-21]. Huang et al. [22] proposed a bidirectional evolutionary structural optimization (BESO) method to optimize the distribution of porous materials and composites with periodic micro-structures and maximize the stiffness of macro-structure. Coelho et al. [23] proposed a topology optimization method for three-dimensional (3D) LS, in which the optimization scheme is composed of two main loops, namely, the outer loop solves the macro design of materials while the inner loop uses the homogenization method to optimize the topology of cells.

Above all, most of the methods rely on current topology optimization (TO) methods, including BESO [24], moving morphable component (MMC) [25], and level set-based method (LSM) [26], and many excellent research results have been obtained. However, stress constraint optimization as one of the classical problems in the TO method still faces many challenges, such as singularity phenomenon and local optimal solution [19]. On the other hand, the TO methods based on the black box model are difficult to give the explicitly mechanical guidance for the structural optimization [27]. In addition, the traditional solid structures usually contain some material redundancy regions and complex features such as corners and lightening holes. The mechanical performances of LS, designed by directly filling the unit cells in the design domain of the solid structures, are constrained by the external shape, which can be improved.

Load path [28, 29] is a concept for tracking transferred load within a structure starting from loading points and ending at supporting points, which has been studied in structural design in recent years [30-32]. Kelly et al. [33-34] inspired by the balance characteristics of fluid stream tube, proposed a load path method based on the equilibrium principle of stress components. The method has been extended to load paths visualization of 3D models and

applied to the design of an aircraft wing spoiler and fiber steered composite [35-37]. The advantage of this method is that it can give clear load paths in a given structure and provide guidance for the performance analysis of the local region. In this study, a new design and optimization method based on the theory of load paths for the variable-density LS is proposed, which can optimize the external shape and internal unit cells simultaneously.

The outstanding contributions of this paper include the following: (1) the design criteria of external shape are established based on the principle of smoother load paths in the structure. (2) An index of load flow capacity S is defined to indicate the load paths density and control the density distribution of unit cells for the LS. (3) The detailed optimization strategy of internal unit cells including mathematical model and algorithm is given to realize the structural lightweight. This paper is structured as follows: Section 2 describes the proposed method including four steps, and the detailed process of each step is described. In Section 3, three examples of a cantilever plate, an L-shaped bracket as well as a classical three-point bending beam are used to verify the proposed method by numerical simulation or experiment. Section 4 concludes our work.

2. METHODOLOGY

The proposed method consists of four steps, as shown in Fig. 1. First, the envelope model of a given structure is established according to the working conditions and functional features (Step 1). Then, the Finite Element Model (FEM) is established and the load paths are visualized by the load path theory (Step 2). Next, the design criteria of external shape are established by analyzing the load transferred law (Step 3). Finally, an index of load flow capacity S is constructed and the optimization strategy and algorithm of variable-density unit cells are given (Step 4). The detailed design process of each step is described in this section, and three examples are used to verify the proposed method in next section.

2.1 Establishment of Envelope Model

The traditional structures usually contain features such as corners and lightening holes, which may interfere with the direction of load paths. It is necessary to abandon these features designed by traditional design methods. So, the envelope model of a given structure is firstly established in this method by analyzing the working conditions and functional features. The basic criteria [38] are as follows: (1) the working conditions of the parts are analyzed to ensure that the constrained and loaded regions remain unchanged. (2) The internal regions and functions are analyzed and the internal holes that do not affect the normal work are filled. (3) The outer boundary of the parts is analyzed and the complex boundary is filled into the regular boundary.

2.2 Load paths visualization

The theory of load path visualization is described in [34]. A hypothetical force stream tube is introduced as shown in Fig. 2; the load paths are defined as curves that surround stream tube where the force remains constant. The tube inherits properties similar to that of a fluid stream tube in that no force (fluid) crosses the boundaries and the magnitude of the forces at the ends are such that equilibrium is satisfied over the tube, i.e.

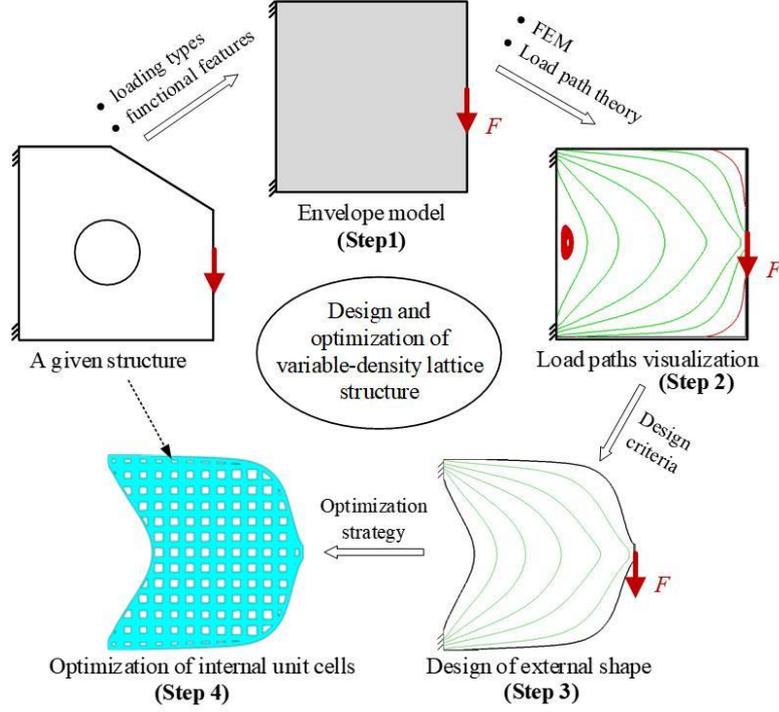$$F_a = F_b \ . \tag{1}$$

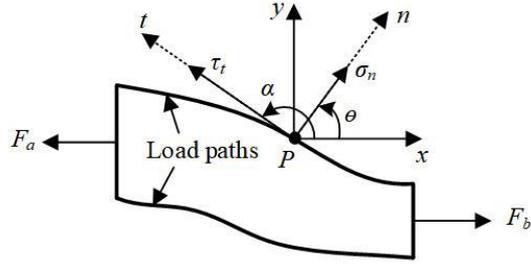**Fig. 1** Design and optimization method based on load paths

Fig. 2 Schematic diagram of the force stream tube

For arbitrary point P on the pipe wall, there are a normal stress σ_n and a shear stress τ_t. According to the principle of force equilibrium, the stress components at point P satisfy Eq. (2).

$$\begin{cases} \sigma_n \cos\theta - \tau_t \sin\theta = 0 \ (x\text{-direction}) \\ \sigma_n \sin\theta - \tau_t \cos\theta = 0 \ (y\text{-direction}) \end{cases} . \tag{2}$$

Angle α and θ is taken as the direction of load path and the normal line at point P. For a 3D structure, the stress components at a point form a second order tensor; it can be represented in a [3×3] matrix. If each row gives three stresses acting on a plane that the normal is aligned with one of the coordinate axes, then

$$[\sigma] = \begin{bmatrix} \sigma_{xx} & \sigma_{xy} & \sigma_{xz} \\ \sigma_{yx} & \sigma_{yy} & \sigma_{yz} \\ \sigma_{zx} & \sigma_{zy} & \sigma_{zz} \end{bmatrix},$$ (3)

Where, σ_{xy} is the shear stress acting on the plane that the normal is in the x direction and pointing y direction. Eigenvalues and eigenvectors of this matrix provide the principal stresses and principal stress vectors.

Load paths can be defined by plotting contours aligned with total stress pointing vectors given by the columns of the stress matrix. Each column of the matrix gives the stress component in the corresponding coordinate direction on the three planes that form the sides of the corner element depicted in Fig. 3.
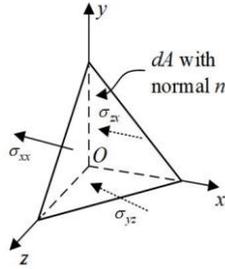

Fig. 3 Construct for force component

The pointing stress vectors are thus defined at every point in the domain by

$$\begin{cases} V_x = \sigma_x i + \tau_{yx} j + \tau_{zx} k \\ V_y = \tau_{xy} i + \sigma_y j + \tau_{zy} k \\ V_z = \tau_{xz} i + \tau_{yz} j + \sigma_z k \end{cases}.$$ (4)

Using the pointing stress vector, the force acting on the infinitesimal element can be described as the vector dot product:

$$\begin{cases} F_x = \int V_x \cdot \vec{n} \, dA \\ F_y = \int V_y \cdot \vec{n} \, dA \\ F_z = \int V_z \cdot \vec{n} \, dA \end{cases}.$$ (5)

Normal $\vec{n} = n_x \boldsymbol{i} + n_y \boldsymbol{j} + n_z \boldsymbol{k}$. Since the force in x-direction along the curves is zero, it is required that normal $\vec{n}$ is perpendicular to pointing stress vector V_x along the curves.

Therefore, the load paths are described by the sequential connection of the pointing stress vectors. Three pointing stress vectors (V_x, V_y and V_z) are defined, and they describe the load paths in the corresponding direction.

The stress components can be solved based on the FEM and the direction of load paths in each element can be calculated using Eq.(1) and Eq.(5). The nodes and elements information, including node number, coordinates and stress components, are extracted in ANSYS 18.0. The load paths can be fitted in the post-processing software TECPLOT by importing the stress information.

2.3 Design criteria of external shape

The external shape of the envelope model is usually designed as regular shape, resulting in some material redundancy regions or stress concentration regions in the structure. Generally, the features of chamfer, fillet or hole are used to improve the stress state of these regions, but there is a lack of mechanical theory guidance. The load paths can directly reflect the load transferred law and provide guidance for shape design. Waldman et al. [34, 39] found that the stresses are low and the normalized pointing vectors show re-circulating structures or "eddies", as shown in Fig. 4. The force flow patterns arise because of the requirements of equilibrium, and it is suggested that the regions occupied by these eddies can be removed in the process of design.
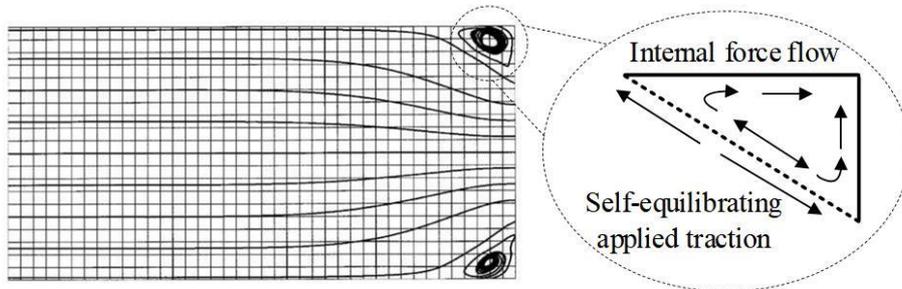

Fig. 4 Formation of eddies in low stress regions

On the other hand, the discontinuous load paths are easily found (Region 1 in Fig. 5). The corresponding regions are considered that the load transfer is blocked by the structural shape and more materials should be added. In addition, there are some regions where the load does not pass through at the corner of the structure (shown in Region 2 in Fig. 5), it is suggested to remove the supplementary materials or replaced by other features, such as fillet, chamfer.

Based on the above analysis, the design criteria of external shape are established as follows: the regions with eddies or where the force does not pass should be removed, or replaced by the features of filled, chamfer, as well as hole. More materials should be added in the regions with discontinuous load paths. The functional requirements of the part should be considered in the process of design and the general principle is to arrange the materials along the load paths as much as possible.
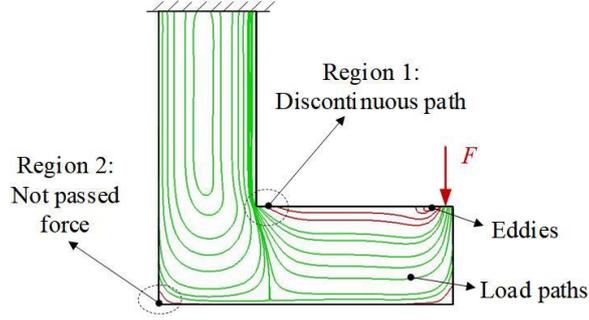
Fig. 5 Other features of load paths in an L-shaped plate

2.4 Optimization strategy of internal unit cells

2.4.1 Load flow capacity S

The density of load paths reflects the magnitude of loads in the local regions, which can be used to guide the distribution law of internal unit cells of lattice structure and improve the mechanical performances. There are several load flow fields in the structure with balanced force, and any load stream tube with different cross sections can be randomly selected in the fields. As shown in Fig. 6, the cross-sectional areas of two ends of a force stream tube are A_1 and A_2, respectively. Then, a small load flow channel is selected inside the tube, and the cross-sectional areas of the two ends are assumed to be dA_1 and dA_2. According to the theory of load paths and the principle of force equilibrium, the internal forces of two small cross-sections of load flow channel are equal in the x-direction. So,

$$p_{x1}dA_1 = p_{x2}dA_2, \tag{6}$$

Where p_{x1} and p_{x2} are the stress components of regions dA_1 and dA_2 along x-direction.
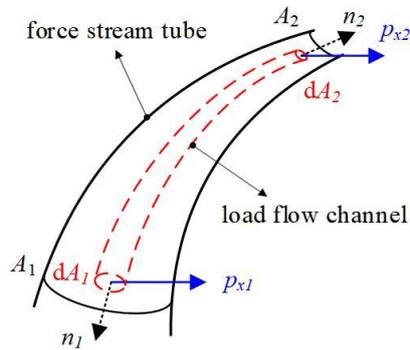

Fig. 6 Schematic diagram of internal load flow

The entire force stream tube is a collection of load flow channels, and the internal forces of force stream tube along x-direction can be integrated as shown in Eq. (7).

$$\int_{A_1} p_{x1} dA_1 = \int_{A_2} p_{x2} dA_2 . \tag{7}$$

Thus, the internal forces through each cross section is equal to that in any other cross section in a force-balanced structure, and the cross-sectional area is inversely proportional to the stress components distributed on the surface. It is assumed that the transferred loads at the unit cross section BC of load flow channel is p, and the length $l=1$, as shown in Fig. 7. The components along the coordinate axis are represented by p_x and p_y. Based on the equilibrium principle, we have

$$\begin{cases} p_{x1} = \sigma_x \cos\theta + \tau_{yx} \sin\theta \\ p_{y1} = \sigma_y \sin\theta + \tau_{xy} \cos\theta \end{cases} . \tag{8}$$
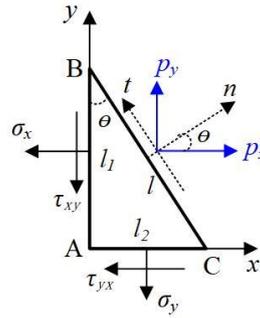

Fig. 7 Internal force decomposition at unit cross section

By substituting Eq. (8) into Eq. (7), we get

$$\int_{A_1} (\sigma_{x1} \cos\theta_1 + \tau_{yx1} \sin\theta_1) dA_1 = \int_{A2} (\sigma_{x2} \cos\theta_2 + \tau_{yx2} \sin\theta_2) dA_2 . \tag{9}$$

According to the geometric relationship in Fig. 7, Eq. (9) can be simplified as

$$\int_{A_1} \sqrt{\sigma_{x1}^2 + \tau_{yx1}^2} \, dA_1 = \int_{A2} \sqrt{\sigma_{x2}^2 + \tau_{yx2}^2} \, dA_2 . \tag{10}$$

Similarly, the entire force flow tube in the y-direction can be written as follows:

$$\int_{A_1} \sqrt{\tau_{xy1}^2 + \sigma_{y1}^2} \, dA_1 = \int_{A2} \sqrt{\tau_{xy2}^2 + \sigma_{y2}^2} \, dA_2 . \tag{11}$$

Based on the principle of internal force continuity, the internal force values are constant for all load paths and can be explicitly expressed. The component of the transferred loads in x-direction is represented by σ_x and τ_{xy}, while the component in y-direction is represented by σ_y and τ_{xy}. The vector sum is defined as load flow capacity S, which can be expressed as

$$S = \sqrt{\sigma_x^2 + 2\tau_{xy}^2 + \sigma_y^2} . \tag{12}$$

Load flow capacity S reflects the characteristics of load paths distribution for each direction in a given structure. The magnitude of S for any point in the structure indicates the load paths density. For a large S value, the load paths are relatively dense in the point, otherwise the opposite. So, load flow capacity S can be used to control the density distribution of unit cells for the LS.

2.4.2 Optimization algorithm

The load paths objectively describe the load transferred law in the structure. The load paths in an ideal load-bearing structure will be evenly distributed, and the uneven load distribution is likely to cause stress concentration. So, the optimization criterion is that if the S value in some regions is large, the corresponding density of internal unit cells needs to be increased in order to improve the structural load-bearing performance.

A cross-cell structure is selected and the length of four sides is taken as the design variables to update the dimensions of unit cells, as illustrated in Fig 8. $D_{I,J}$ is the length of unit cell at the I-th row and J-th column, and the shared edge of two adjacent unit cells is determined by average side length, which can effectively avoid the step phenomenon, also known as stress concentration caused by the dimension difference between the adjacent unit cells.
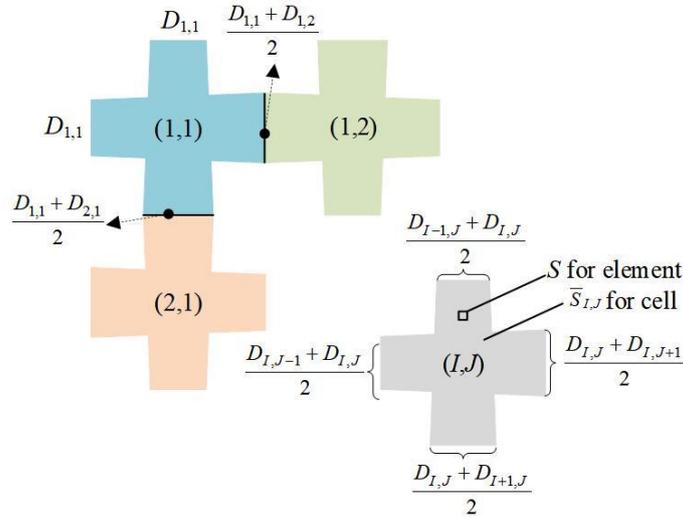

Fig. 8 Variable-density strategy of internal unit cells

The detailed optimization algorithm of variable-density lattice structure is as follows:

(1) Side length $D_{I,J}$ of the unit cells is used as the design variable, and the variation range is set that has an upper limit of D_{max} and a lower limit of D_{min}. The initial value of side length is set as D_{max}.

(2) The stress values at the node of FEM are extracted, and the stress components at the element centroid are calculated by interpolation, and the value of load flow capacity S_i for all elements is obtained by Eq. (12).

(3) The average value of load flow capacity for internal unit cells of a given lattice structure is calculated using

$$\overline{S_{I,J}} = \frac{\sum\limits_{m=1}^{n} S_i}{n} ,$$ (13)

where n is the number of elements for unit cell.

(4) Side length $D_{I,J}$ of the unit cell is calculated by Eq. (14). The maximum value of load flow capacity in all unit cells is denoted as S_{max}. f is the volume fraction, which is used to control the global density of unit cells. If $D_{I,J} > D_{max}$, then $D_{I,J} = D_{max}$; if $D_{I,J} < D_{min}$, then $D_{I,J} = D_{min}$.

$$D_{I,J} = D_{max} \cdot \frac{\overline{S_{I,J}}}{f \cdot S_{max}} .$$ (14)

(5) The density value obtained in step (4) is then assigned to the corresponding unit cell, and the loop iteration is performed until convergence is reached. If the change rate of volume is less than R, it is regarded as convergence, as shown in Eq. (15).

$$\frac{\left| V^{(k+1)} - V^k \right|}{V^k} \le R ,$$ (15)

where k represents the number of iterations, V^k is the volume of the k-th iteration step. R represents the change rate of volume, which is set to 0.01 in this study.

Finally, the optimization model is established as shown in Eq. (16).

$$\begin{cases} \text{Find} & D_{I,J} \\ \text{objective} & (\left| V^{(k+1)} - V^k \right| / V^k) \le R \\ \text{subject to} & D_{I,J} = D_{max} \cdot \overline{S_{I,J}} / (f \cdot S_{max}) \\ & \overline{S_{I,J}} = (\sum\limits_{m=1}^{n} S_i) / n \\ & S_i = \sqrt{\sigma_{xi}^2 + 2\tau_{xyi}^2 + \sigma_{yi}^2} \\ & F = KU \end{cases} ,$$ (16)

where, U, F, K are the displacement vector, force vector, and stiffness matrix.

3. EXAMPLES

In this section, three examples, including a cantilever plate, an L-shaped bracket as well as a classical three-point bending beam are designed and optimized by the proposed method.

3.1 Cantilever plate

The problem setting of a square cantilever plate is illustrated in Fig. 9 with an area of 60×60 mm^2 and a thickness of 1 mm. The left top and left bottom edge corners are constrained and a vertical load F is applied at the middle of the right edge. The vertical load is distributed over 5 nodes to avoid stress concentration.
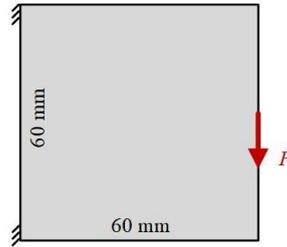

Fig. 9 A square cantilever plate

The FEM is established and the load paths are calculated by the Section 2.2; the results are shown in Fig. 10(a). Region 1 belongs to the region where the loads do not pass, and Region 2 forms the phenomenon of eddies, where the materials can be removed. According to the design criteria in Section 2.3, the materials are arranged along the outermost load path and a new shape with load paths is given in Fig 10(b).
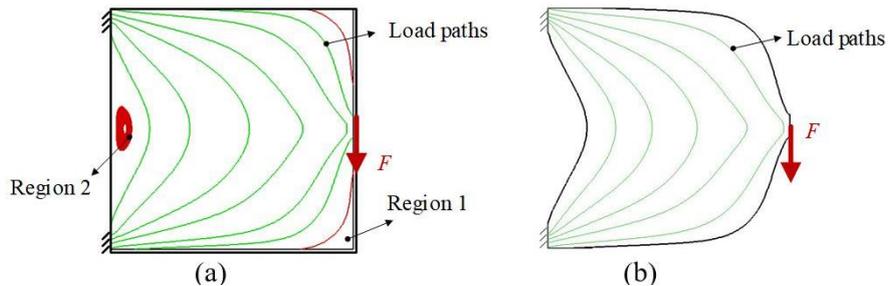

Fig. 10 Load paths visualization of the cantilever plate (a) Load paths of initial shape (b) Load paths of new shape

In order to further verify the rationality of the proposed design criteria of external shape, the stiffness and strength of two models in Fig. 10 are compared by FEA. The boundary conditions and the selected material properties are exactly the same. The element type is solid 185 and the element size is 0.2mm. The FEA results including displacement and stress distribution of initial shape and new shape are shown in Figs. 11 and12.

The results show that the volume of new shape decreases by 22.44%, the maximum displacement decreases from 0.0086 mm to 0.0064 mm, accounting for 34.50%, the maximum stress decreases from 88.83 MPa to 61.08 MPa, accounting for 37.50%. It shows that the mechanical performances of the cantilever plate are improved obviously by retaining the regions with effective load paths and removing the regions with invalid load paths.
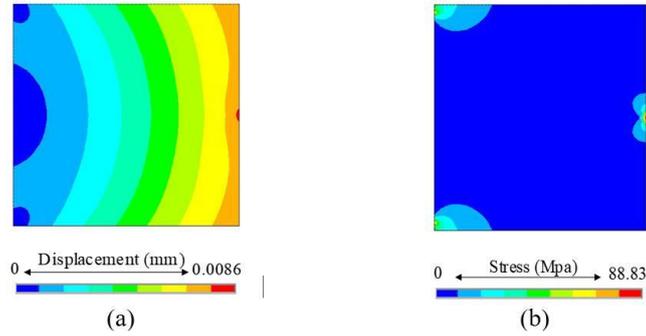
F. WU, H. LIAN, G. PEI, B. GUO, Z WANG

Fig. 11 The FEA results of initial shape of the cantilever plate (a) Displacement distribution (b) Stress distribution

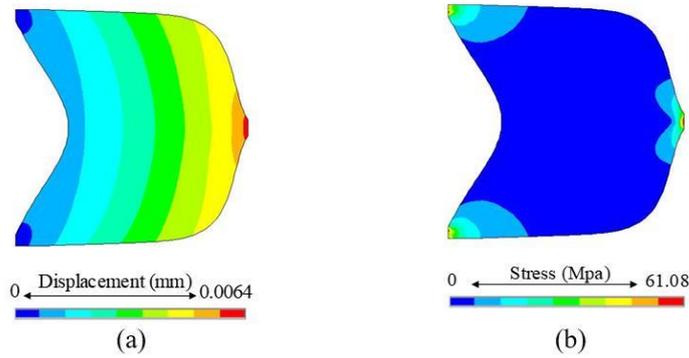**Fig. 12** The FEA results of a new shape of the cantilever plate (a) Displacement distribution (b) Stress distribution

Then, a unit cell of 5×5 mm^2 is selected to fill the inner region of the new shape in Fig. 10b. Considering the accuracy requirements of additive manufacturing technology, D_{min} is set to 0.4 mm and D_{max} is set to 3.0 mm. Volume fraction f is set to 0.5. The unit cells are filled according to the optimization algorithm in Section 2.4 and the model of variable-density lattice structure is established and shown in Fig. 13.
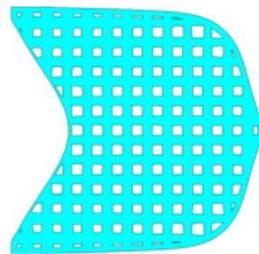

Fig. 13 Variable-density lattice structure of the cantilever plate

The FEA with same loads and constraints is performed to compare the mechanical performance of the variable-density model based on the proposed method (model A1), the variable-density model based on Von Mises stress (model A2), and the uniform-density model (model A3), as shown in Fig. 14. The volume, maximum displacement and maximum Von Mises stress are listed in Table 1. The results show that the maximum displacement and stress of model A1 are smaller than the other two models, and the weight reduction effect is the best, which shows that the proposed design and optimization method has good applicability.
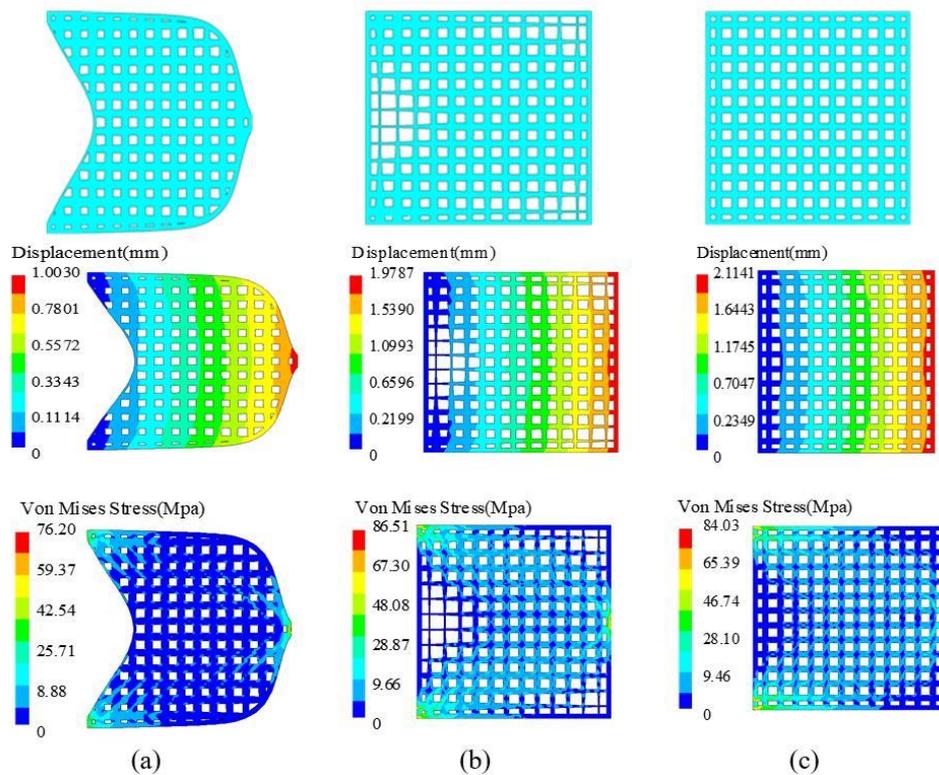

Fig. 14 The comparison of three different cantilever plates (a) model A1 (b) model A2 (c) model A3

Table 1 Results for different cantilever plates

Parameter	model A1	model A2	model A3
Volume (mm^3)	2404	2517	2673
Maximum displacement (mm)	1.00296	1.97867	2.11406
Maximum Von Mises Stress (MPa)	76.7985	86.5097	84.0265

3.2 L-shaped bracket

The second example is an L-shaped bracket as shown in Fig.15; the top edge is constrained and a vertical load F is applied at the middle of the right edge. The load paths are calculated by the Section 2.2 as shown in Fig. 16. Region 1 belongs to the region where the loads do not pass, and Region 2 forms the phenomenon of eddies, where the materials can be removed. The discontinuous load paths are found in Region 3, and more materials should be added.
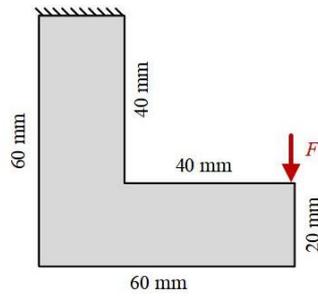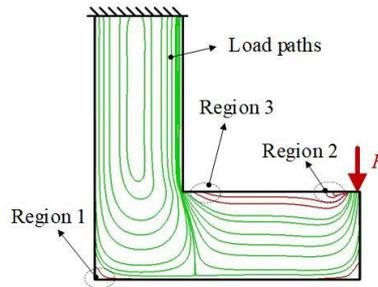

Fig. 15 L-shaped bracket

Fig. 16 Load paths of L-shaped bracket

On this basis, the same size of unit cell, value of D_{max}, D_{min}, and volume fraction f are set with the example of cantilever plate, the optimization of unit cells density is carried out. The new model is established as shown in Fig. 17.
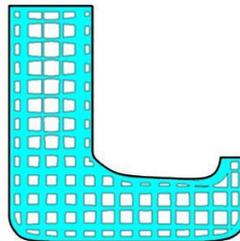

Fig. 17 The lattice structure of L-shaped bracket

Similarity, the FEA with same loads and constraints is performed to compare the performance of variable-density model based on the proposed method (model B1), the variable-density model based on Von Mises stress (model B2), and the uniform-density model (model B3), as shown in Fig. 18. The volume, maximum displacement and maximum stress are listed in Table 2. The results show that the maximum displacement and stress of model B1 are smaller than the other two models, and the weight reduction effect is the best.
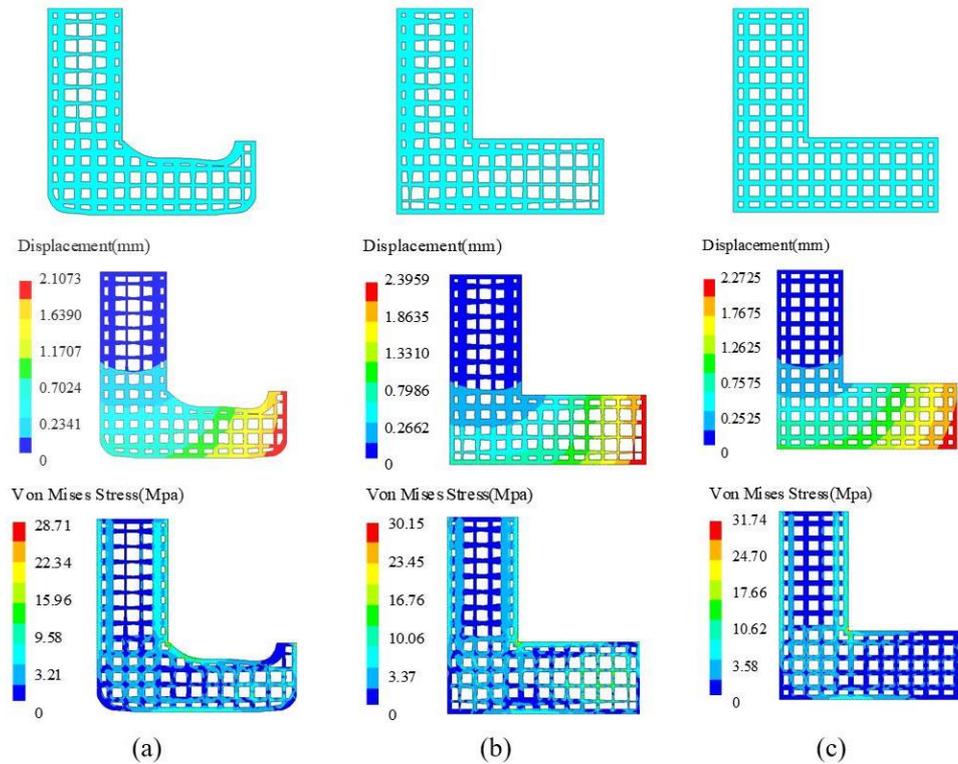

Fig. 18 The comparison of three different L-shaped brackets (a) model B1 (b) model B2 (c) model B3

Table 2 Results for different L-shaped brackets

Parameter	model B1	model B2	model B3
Volume (mm^3)	1391	1466	1498
Maximum displacement (mm)	2.1073	2.3959	2.2725
Maximum Von Mises Stress (MPa)	28.71	30.15	31.74

3.3 Three-point bending beam

The third example is a three-point bending beam and the length, width and height are 100×20×25 mm, as shown in Fig. 19. The upper platform has a width of 20 mm, and each lower platform has a width of 15 mm. A load is applied to the upper surface, and two fixed constraints are applied to the lower surface.
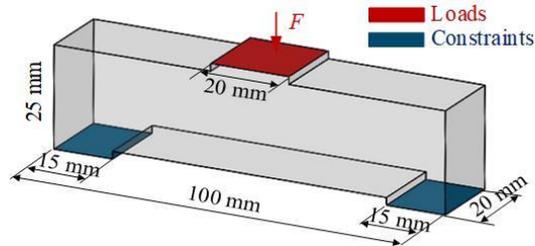

Fig. 19 The structure of three-point bending beam

The load paths of cross-section in front view are calculated by Section 2.2 as shown in Fig. 20. The regions with eddies and where the loads do not pass are removed. The same size of unit cell, value of D_{max}, D_{min}, and volume fraction f are set with the example of cantilever plate, the optimization of unit cells density is carried out. A new three-point bending beam is established as shown in Fig. 21.
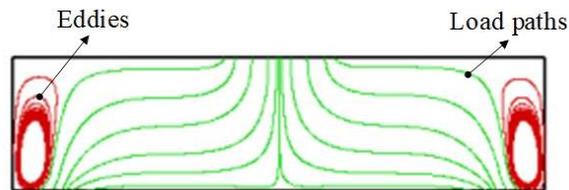

Fig. 20 Load paths visualization of cross-section in front view
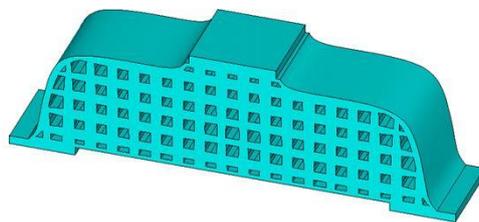

Fig. 21 A new three-point bending beam with unit cells

In order to further verify the proposed method, a group of physical models was fabricated by a 3D pro X3 printer using poly-lactic acid (PLA). The variable-density bending beams based on stress (model C2) and the uniform-density bending beams (model C3) are designed and fabricated using the same device, as shown in Fig. 22.
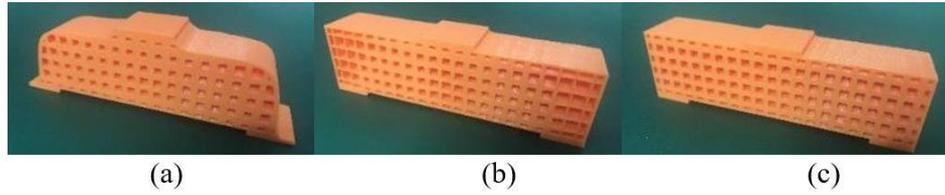
Fig. 22 Physical models of different three-point bending beam (a) Model C1 (b) Model C2 (c) Model C3.

The experiment was carried out using a microcomputer-controlled electronic universal testing machine. The linear displacement with 1 mm/min was applied; the displacement and corresponding loads were recorded by the data acquisition system. Three groups of experiments were carried out on each model to assure that the experiments are fulfilling the repeatability conditions and the results are not under the influence of exceptional characteristics or flaws of a single sample. The experimental results are shown in Fig. 23.
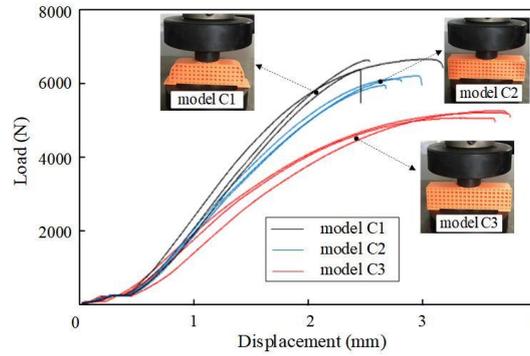

Fig. 23 Experimental results of three groups of physical models

The comparison of volumes, manufacturing times, ultimate loads is listed in Table 3. Two variable-density bending beams (model C1 and model C2) show the significant advantages compared to the uniform-density bending beam (model C3). Compared with the variable-density model C2 based on stress, the volume of the new model C1 is further reduced by 6.13%, the printing time is reduced by 11.65%, but the average ultimate load is increased by 7.56%. These results show that the mechanical performances of variable-density lattice structure designed by the proposed method are significantly improved. And the material usage and printing time are reduced.

Table 3 Performance comparison of three models

Parameter	model C1	model C2	model C3
Volume (mm^3)	33540	35730	39080
Fabrication time (min)	364	412	443
Average ultimate load (N)	6922.9	6436.2	5463.4

4. Conclusion

A novel design and optimization method of variable-density LS is proposed to optimize the external shape and internal unit cells simultaneously in this paper. The method is divided into four steps, as follows: Step1, the envelope model of any given structure is established according to the working conditions and functional features; Step2, the load paths are visualized by the load path theory; Step3, the external shape is re-designed by analyzing the load transferred law; Step4, the distribution of internal unit cells is optimized according to the dense of load paths. Three examples of a cantilever plate, an L-shaped bracket and a classical three-point bending beam are used to verify the proposed method by numerical simulation or experiment. The results show that the models designed by the proposed method have better mechanical performances, lower material usage and less printing time. The major contributions of this work can be summarized as follows:

(1) The design criteria of external shape are established based on the principle of smoother load paths in the structure, which give the designers a straightforward optimization suggestion.

(2) A new index of load flow capacity S is defined to indicate the load paths density and control the density distribution of unit cells.

(3) The detailed optimization strategy of internal unit cells including mathematical model and algorithm is given to realize the structural lightweight.

(4) The external shape and internal unit cells for a given structure are optimized simultaneously for the first time.

References

1. Wang, Y., Li, S.S., Yu, Y., Xin, Y.M., Zhang, X.Y., Zhang, Q., Wang, S., 2018, *Lattice structure design optimization coupling anisotropy and constraints of additive manufacturing*, Materials & Design, 196, 109089.
2. Helou, M., Kara, S., 2018, *Design, analysis and manufacturing of lattice structures: an overview*, International Journal of Computer Integrated Manufacturing, 31(3), pp. 243-261.
3. Panesar, A., Abdi, M., Hickman, D., Ashcroft, I., 2018, *Strategies for functionally graded lattice structures derived using topology optimisation for additive manufacturing*, Additive Manufacturing, 19, PP. 81-94.
4. Wu, J., Aage, N., Westermann, R., Sigmund, O., 2017, *Infill optimization for additive manufacturing approaching bone-like porous structures*, IEEE Transactions on Visualization and Computer Graphics, 24(2), pp. 1127-1140.
5. Alzahrani, M., Choi, S.K., Rosen, D.W., 2015, *Design of truss-like cellular structures using relative density mapping method*, Materials & Design, 85(15), pp. 349-360.
6. Choy, S.Y., Sun, C.N., Leong, K.F., Wei, J., 2017, *Compressive properties of Ti-6Al-4V lattice structures fabricated by selective laser melting: design, orientation and density*, Additive Manufacturing, 16(1), pp. 213-224.
7. Liu, J., Gaynor, A.T., Chen, S., Kang, Z., Suresh, K., Takezawa, A., Li, L., Kato, J., Tang, J., Wang, C.C.L., Cheng, L., Liang, X., To, A.C., 2018, *Current and future trends in topology optimization for additive manufacturing*, Structural and Multidisciplinary Optimization, 57(2), pp. 2457-2483.

8. Cheng, L., Zhang, P., Biyikli, E., Bai, J.X., Robbins, J., To, A.C., 2017, *Efficient design optimization of variable-density cellular structures for additive manufacturing: theory and experimental validation*, Rapid Prototyping Journal, 23(4), pp. 660-677.

9. Smith, M., Guan, Z., Cantwell, W.J., 2013, *Finite element modelling of the compressive response of lattice structures manufactured using the selective laser melting technique*, International Journal of Mechanical Sciences, 67(1), pp. 28-41.

10. Strzalka, C., Marinkovic, D., Zehn, M.W., 2021, *Stress mode superposition for a priori detection of highly stressed areas: mode normalisation and loading influence*, Journal of Applied and Computational Mechanics, 7(3), pp. 1698-1709.

11. Strzalka, C., Zehn , M., 2020, *The influence of loading position in a priori high stress detection using mode superposition*, Reports in Mechanical Engineering, 1(1), pp. 93-102.

12. Chen, W., Xia, L., Yang, J., Huang, X., 2018, *Optimal microstructures of elastoplastic cellular materials under various macroscopic strains*, Mechanics of Materials, 118, pp. 120-132.

13. Savio, G., Meneghello, R., Concheri, G., 2016, *Optimization of lattice structures for additive manufacturing technologies*, Advances on Mechanics, Design Engineering and Manufacturing, 9, pp. 213-222.

14. Liu, C., Du, Z., Zhang, W., Guo, X., 2017, *Additive manufacturing oriented design of graded lattice structures through explicit topology optimization*, Journal of Applied Mechanics, 84(8), 081008.

15. Groen, J., Sigmund, O., 2017, *Homogenization-based topology optimization for high-resolution manufacturable microstructures*, International Journal for Numerical Methods in Engineering, 113(8), pp. 1148-1163.

16. Chu, C., Graf, G., Rosen, D.W., 2013, *Design for additive manufacturing of cellular structures*, Computer Aided Design and Applications, 5(5), pp. 686-696.

17. Nguyen, J., Park, S.I., Rosen, D., 2013, *Heuristic optimization method for cellular structure design of light weight components*, International Journal of Precision Engineering and Manufacturing, 14(6), pp. 1071-1078.

18. Zhang, P., Toman, J., Yu, Y.Q., Biyikli, E., Kirca, M., Chmielus, M., To, A.C., 2015, *Efficient design-optimization of variable-density hexagonal cellular structure by additive manufacturing: theory and validation*, Journal of Manufacturing Science and Engineering, 137, 021004.

19. Cheng, L., Bai, J.X., To, A.C., 2019, *Functionally graded lattice structure topology optimization for the design of additive manufactured components with stress constraints*, Computer Methods in Applied Mechanics and Engineering, 344, pp. 334-359.

20. Cheng, L., Liu, J., To, A.C., 2018, *Concurrent lattice infill with feature evolution optimization for additive manufactured heat conduction design*, Structural and Multidisciplinary Optimization, 58(2), pp. 511-535.

21. Wang, X., Zhang, P., Ludwick, S., Belski, E., To, A.C., 2018, *Natural frequency optimization of 3D printed variable-density honeycomb structure via a homogenization-based approach*, Additive Manufacturing, 20, pp. 189-198.

22. Huang, X., Zhou, S.W., Xie, Y.M., Li, Q., 2013, *Topology optimization of microstructures of cellular materials and composites for macrostructures*, Computational Materials Science, 67, pp. 397-407.

23. Coelho, P.G., Amiano, L.D., Guedes, J.M., Rodrigues, H.C., 2016, *Scale-size effects analysis of optimal periodic material microstructures designed by the inverse homogenization method*, Computurs & Structures, 174(10), pp. 21-32.

24. Huang, X., Xie, Y., 2010, *A further review of ESO type methods for topology optimization*, Structural and Multidisciplinary Optimization, 41, pp. 671-683.

25. Zhang, W., Yuan, J., Zhang, J., Guo, X., 2016, *A new topology optimization approach based on Moving Morphable Components (MMC) and theersatz material model*, Structural and Multidisciplinary Optimization, 53(6), pp. 1243-1260.

26. Allaire, G., Jouve, F., Toader, A.M., 2004, *Structural optimization using sensitivity analysis and a level-set method*, Journal of Computational Physics, 194(1), pp. 363-393.

27. Suzuki, T., Fukushige, S., Tsunori, M., 2020, *Load path visualization and fiber trajectory optimization for additive manufacturing of composites*, Additive Manufacturing, 31, 100942.

28. Zhao, S., Mao, L., Wu, N., Karnaoukh, S., 2022, *Load path visualization using u* index and principal load path determination in thin-walled structures*, Facta Universitatis-Series Mechanical Engineering, doi: 10.22190/FUME211105006Z.

29. Wu, F., Wang, Z., Song, D., Lian, H., 2022, *Lightweight design of control arm combining load path analysis and biological characteristics*, Reports in Mechanical Engineering, 3(1), pp. 71-82.

30. Wang, Q.G., Zhang, G., Sun, C., Wu, N., 2019, *High efficient load paths analysis with U* index generated by deep learning*, Computer Methods in Applied Mechanics and Engineering, 344, pp. 499-511.

31. Tamijani, A., Gharibi, K., Kobayashi, M., Kolonay, R., 2018, *Load paths visualization in plane elasticity using load function method*, International Journal of Solids and Structures, 135, pp. 99-109.

32. Takahashi, K., Omiya, M., Iso, T., Zaiki, Y., Sakurai, T., Maki, T., Urushiyama, Y., Naito, T., 2013, *Load transfer ustar (U*) calculation in structures under dynamic loading*, Transactions of the Japan Society of Mechanical Engineers, Part A, 79(807), pp. 1657-1668.
33. Kelly, D.W., Elsley, M., 1995, *A procedure for determining load paths in elastic continua*, Engineering Computations, 12(5), pp. 415-424.
34. Kelly, D.W., Hsu, P., Asudullah, M., 2001, *Load paths and load flow in finite element analysis*, Engineering Computations, 18(1/2), pp. 304-313.
35. Tosh, M.W., Kelly, D.W., 2000, *On the design, manufacture and testing of trajectorial fibre steering for carbon fibre composite laminates*, Composites Part A: Applied Science and Manufacturing, 31(10), pp. 1047-1060.
36. Kelly, D.W., Reidsema, C., Lee, M., 2010, *On load paths and load bearing topology from finite element analysis*, IOP Conference Series: Materials Science and Engineering, 10(1), pp. 51-54.
37. Zhao, J., Li, B.T., Gao, X., Zhen, Y., Hua, Y., 2013, *Research on the load-bearing characteristics of complex structural components based on the representation of load paths*, IEEE International Symposium on Assembly & Manufacturing, IEEE, 2013, pp. 176-179.
38. Wang, Z.H., Wu, N., Wang, Q.G., Guo, B.S., Wu, F.H., 2020, *Novel bionic design method for skeleton structures based on load path analysis*, Applied Sciences-Basel, 10(22), 8251
39. Waldman, W., Heller, M., Rose, F., 2002, *Advances in two dimensional structural load flow visualisation*, Engineering Computations, 19(3), pp. 305-326.